PROCEEDINGS, 47th Workshop on Geothermal Reservoir Engineering
Stanford University, Stanford, California, February 7-9, 2022
SGP-TR-223

Hydro-Mechanical Modeling of Magma Injections in NE Sector of Mutnovsky Volcano (Kamchatka)

Alexey Kiryukhin[1], Noriyoshi Tsuchiya[2]

1 - Institute of Volcanology & Seismology FEB RAS, Piip 9, Petropavlovsk-Kamchatsky 683006, Russia

2 - Graduate School of Environmental Studies, Geomaterial and Energy Lab., Tohoku University, Sendai 980-8579, Japan

avkiryukhin2@mail.ru

Keywords: magma, fracking, Mutnovsky, volcano, MEQ, production, reservoirs, supercritical, reservoir

ABSTRACT

Magma-hydrothermal system developed multiple geothermal resources, coupled with conventional and supercritical geothermal reservoirs. MEQs and resistivity by MT measurement can indicate potential of deep-seated supercritical (or superhot) geothermal reservoir. Mutnovsky geothermal field is a largest electricity producer in Kamchatka (62 MWe installed in 2002), while power production was not extended since that time, focusing on existing Dachny production reservoir re-drilling activity. NE Mutnovsky volcano sector, where significant magma fracking activity was revealed based on MEQ data, is adjacent to Dachny. Thus we performed CFRAC hydromechanical modeling to better understand fracking properties of potential production geothermal reservoir above mentioned. Hydromechanical modeling also aiming to estimate relationship between MEQ's magnitudes and magma/gas injection volumes. Those fracking properties are crucial to be used for subsequent heat transfer modeling of potential production geothermal reservoirs.

1. INTRODUCTION

We are conducting supercritical geothermal project, and deep drilling project named as "Japan Beyond Brittle Project"(JBBP) The temperatures of geothermal fields operating in Japan and Kamchatka range from 200 to 300°C (average ~250°C), and the depths range from 1000 to 2000 m (average ~1500 m). In conventional geothermal reservoirs, the mechanical behavior of the rocks is presumed to be brittle, and convection of the hydrothermal fluid through existing network is the main method of circulation in the reservoir. In order to minimize induced seismicity, a rock mass that is "beyond brittle" is one possible candidate, because the rock mechanics of "beyond brittle" material is one of plastic deformation rather than brittle failure. In that case, the main points for development of supercritical geothermal reservoir is to maintain high permeability of the reservoir even in beyond brittle condition.

The presence of supercritical fluids with temperatures of ~400–500◦C has been discovered from several active geothermal fields around the world indicated that there is available permeability in such a reservoir. To understand the geological and development models of a Supercritical ("Beyond Brittle" and/or "Superhot") geothermal reservoir, geological survey of granite–porphyry system was performed. In order to reveal geological model, the granite–porphyry system provides useful information for creation of fracture clouds in supercritical geothermal reservoirs.

A high silicification zone that was observed at the top of granite intrusion. The earlier generation of quartz had the highest temperature and Ti content (516−640°C; Ti = ~8−37 ppm) and was characterized by high luminescence and intensive brittle failure. The characteristics and temperature were similar to that quartz phenocryst in the crystalline granodiorite (531−793°C; Ti = ~10−140 ppm), suggested being the relic of quartz phenocryst during the magmatic stage. The second and third generation of quartz had a weak to dark luminesce and lower temperature (375−465°C) and was formed as overgrowth and a filling of microfractures and cavities of the earlier quartz generation. The quartz was generated during the earlier and higher temperatures of silicification, and therefore potential to be the cap−rock for a supercritical geothermal system.

Granite hosted supercritical geothermal reservoir has been discovered in Kakkonda Geothermal Field trough the deep well (WD-1) which encounter a partly solidified granite with the fluid temperature of >500◦C at the depth of >3 km (Muraoka et al. 1998). It reveals the existence of deep-seated geothermal reservoir beneath the active geothermal field. However, it is challenging to determine the reservoir structure in such a deep environment. The granite-porphyry system recognized as the natural analog for thus reservoir type presenting the condition at the near magma environment (Tsuchiya et al. 2016; Watanabe et al. 2017, 2019; Reinsch et al. 2017).

2. GEOLOGICAL BACKGROUND

Figure 1 shows schematic geological models of magma-hydrothermal regimes for processing in supercritical geothermal reservoirs associated with volcanic activities. Deep magma chamber, which is huge amount of heat source, supplies ascending magma, which is active magma chamber and direct heat source for supercritical and conventional geothermal reservoirs (Amanda et al., 2019). Before eruption, the supercritical resources can exist within granite-porphyry system under cap rock. After eruption, the cap rock is broken and breaching. An active magma can be upwelling through the cap rock and then shallow magma chamber and hydrothermal systems are enhanced within caldera underneath active volcano. Fournier (1999) already mentioned general model of transition from magmatic to epithermal conditions in a subvolcanic environment, where brittle to plastic transition occurs at 370°C to 400°C.

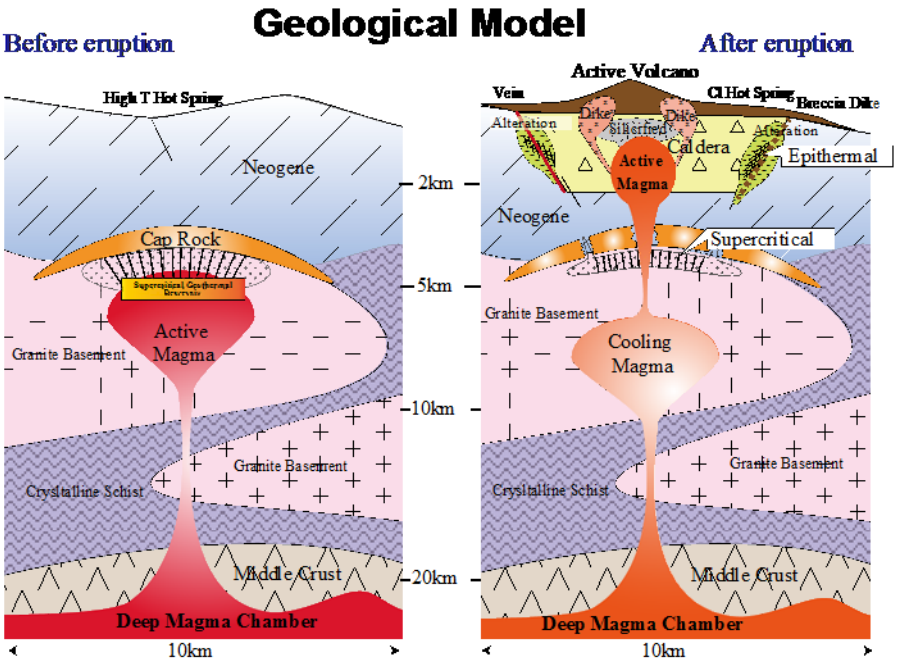

Figure 1: Schematic geological model of supercritical geothermal reservoir

3. SUPERCRITICAL GEOTHERMAL RESOURCES

The granite porphyry system consisted of three main parts based on their textures (crystalline, porphyritic, and silicified). We could say that each part will represent the component of the supercritical geothermal system that depicts the distribution of geothermal components with depth. The thickness of each component and the geothermal gradient were approximated based on the geological map, geobarometry, and geothermometry. The geothermal gradient used in this model was 70°C/km, derived from the temperature and pressure of crystalline granodiorite, assuming that the geothermal gradient was linear. The still molten–partly solidified crystalline granodiorites occupying the system's deepest (core part) appeared as the heat source in the geothermal system. The porphyritic granodiorite embodied the margin of the intrusion (shallower part). This unit intensively was breached by the vein and veinlets, especially as the host of the glassy vein, suggesting the occurrence of high fluid activity, which mimicked the supercritical geothermal reservoir. The accumulation of silica at the top of the intrusion as the silicified zone was potentially the cap–rock of the supercritical geothermal system (Amagai et al., 2019).

The high–temperature silicification stage was represented by the silicified granite. Fluid inclusion and Ti contents showed that this quartz has formed at a similar temperature (~375–465°C), revealing the pressure assumption for fluid inclusion analysis was relevant ~100–200 MPa or 4–7.5 km (lithostatic gradient of 2.7 g/cm^3 crustal density). This depth also coincided with the silica solubility minimum (644 mg/kg H_2O); hydrostatic pressure of 63.7 MPa) at ~6.5 km for the geothermal gradient of 70°C/km (according to Akinfiev and Diamond, 2009). The interval for the caprock was placed at a depth of 6.5–7 km. If we assumed the supercritical reservoir was located just below the cap rocks, the top of the reservoir was around the depth of ~7 km. The thickness of this layer was ~1 km, which made the reservoir at ~7–8 km depth and located at the margin of the granodiorite body (the vein rich–porphyritic–granodiorite), right above crystalline granodiorite in which also coincides with the prior result by Tsuchiya et al. (2016) derived from P-T evolution of a supercritical geothermal reservoir in the study area (at 500–550ºC and ~200 MPa). Therefore, we can assume that the crystalline granodiorite as the heat source was placed at a depth of 8 km and still existed to the depth of 11 km (Fig. 2), which corresponded to the results of Al–in–Hbl geobarometry of crystalline granodiorite (~300 MPa).

.

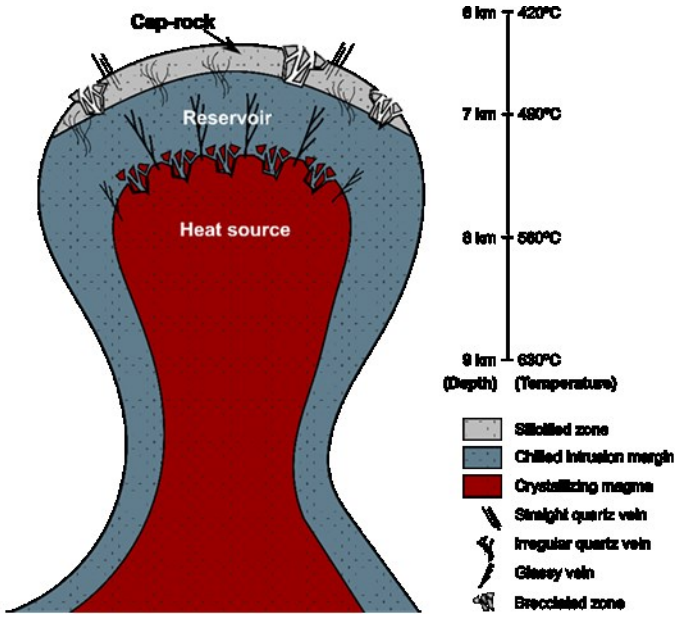

Figure 2: A schematic illustration of the supercritical geothermal structure presents a spatial distribution of the components and veins for the geothermal gradient of 70°C/km. A heat source is a crystalline granodiorite placed at ~8−11 km (~200−300 MPa, ~531−793ºC). The reservoir is located at the margin of the granodiorite body (the vein rich−porphyritic−granodiorite) of ~7−8 km depth (~175−200 MPa, ~500−560ºC). The cap−rock is placed at a depth of 6.5−7 km (~175 MPa, ~430ºC). The high−temperature hydrothermal quartz (~400ºC) is formed during self−sealing and becomes the caprock for the supercritical geothermal system.

4. MODELING MAGMA FRACKING IN CONVENTIONAL HYDROTHERMAL SYSTEMS

4.1 Model Setup

Based on seismic data, let us consider a conceptual model of hydromechanical processes beneath Mutnovsky volcano. We consider a single existing fault in RF geomechanical conditions as the host fault for the injecting dyke (Fig. 3) and apply CFRAC modeling to describe magma injection into it (McClure, 2013, 2014). For the indicated geomechanical conditions, the vertical stress Sv is the minimum, the maximum horizontal stress SH max acts in the NW direction, and the minimum horizontal stress Sh min acts in the NE direction. At a depth of z0 = 4500 m (≈ -3000 m abs.), Sv is estimated as 113.3 MPa (using formula 4.1 and data from Table 4.1, Kiryukhin, 2020); SH max = 279.3 MPa (formula 4.23, where Pp = Pf = 35 MPa design fluid pressure at -3000 m abs, friction coefficient μ = 0.6); Sh min - is taken equal to (Sv + SH max)/2 = 196.3 MPa.

Based on the above, the effective stress tensor under Mutnovsky volcano at a depth of -3000 m abs. in the coordinate system oriented along the main stress directions X, Y, Z (X - SE direction, Y - NE direction, Z - upward direction, see Fig. 3) is written as follows:

$$\sigma_g = \begin{pmatrix} SH_{\max} - Pf & 0 & 0 \\ 0 & Sh_{\min} - Pf & 0 \\ 0 & 0 & Sv - Pf \end{pmatrix} \quad (1)$$

where SH max = 279.3 MPa, Sh min = 196.3 MPa, Sv = 113.3 MPa, Pf = 35 MPa.

The CFRAC program solves a system of hydro-mechanical equations describing flows and deformations in a network of discrete fracture system (McClure, 2014; McClure and Horne, 2013). A double iteration scheme is used in CFRAC, in which the equation for flow is combined with the condition for normal stresses, and shear stresses in the fracture plane form a second system of equations for quasi-static equilibrium conditions. When performing 3D modeling using CFRAC software, the following should be kept in mind: 1) CFRAC in the basic version describes processes in vertical fractures; 2) when describing inclined fractures, it is necessary to rotate the original XYZ coordinate system around the Y axis into a new coordinate system with the Z2 axis in the fracture plane (Y2 = Y); 3) after that, the effective stresses in the new coordinate system X2, Y2, Z2: σ_{xx}, σ_{yy}, σ_{zz}, σ_{xz} and their trends should be redefined.

The CFRAC program defines the threshold values of shear strain rates for earthquake generation as 5 and 2.5 mm/s, respectively (default values of the meqstartvel and meqendvel parameters). At this point, the model element in which the specified condition is reached is interpreted as the initial rupture point, which ends when the shear strain rate falls below the threshold value. Earthquake parameters are identified as follows within the CFRAC program: time, hypocenter coordinates, seismic moments and magnitudes, and rupture areas, and are written to the resulting files.

The seismic moment in CFRAC program M0 is estimated from the shear strain data as follows: $M0 = G \cdot \int \text{slip}\, dA$, where G - shear modulus, A - shear area. Then the magnitude Mw is calculated:

$$Mw = \lg(M_0)/1.5 - 6.06 \quad (2)$$

where M0 is expressed in N · m. In the considered model the static/dynamic option was used: friction coefficient μstatic = 0.6 in absence of rupture, at the beginning of rupture deformation the friction coefficient drops to $\mu_{dynamic}$ = 0.55. In the considered basic modeling scenario, magma injection occurs in a fracture with a dip angle of 30° and dimensions of 4 km (in the dip direction) by 4 km (in the strike direction) with the center of the fracture at a depth of 4500 m (or - 3000 m abs) under the Mutnovsky volcano. In addition, the modeling assumed the following conditions: duration of magma injection from 1 to 30 days, magma flow from 10 to 2000 kg/s, maximum pressure during injection 200 MPa. Physical properties of magma: density 2800 kg/m3, viscosity was set from 9 10^{-5} Pa · s (basalt magma) to 2 Pa · s (andesite magma). Initial magma pressure was set from 5 to 78 MPa, the latter value corresponds to the fluid pressure necessary to activate the fracture according to the Mohr diagram (Fig. 4.18, Kiryukhin, 2020). In addition, other additional scenarios were considered on the model, with the parameters specified in Table 1.

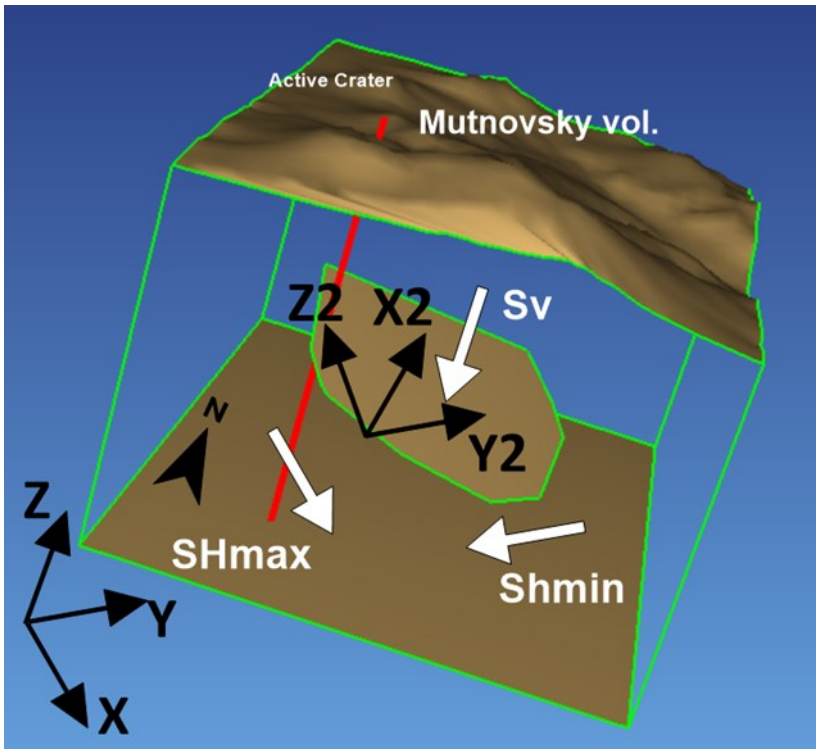

Figure 3: A conceptual model of the geomechanical state during dike injection beneath Mutnovsky volcano. Sv - vertical stress, SH max - maximum horizontal stress, Sh min - minimum horizontal stress.

The effective stress tensor σf in the dyke-fracture coordinate system (X2 - rotation of the X axis around the Y axis by an angle β = 60°, Y2 = Y) was calculated (in MPa) using the known effective stress tensor in the main stress coordinate system (1) using the coordinate transformation matrix:

$$A = \begin{pmatrix} \cos(\beta)*\cos(\alpha) & -\cos(\beta)*\sin(\alpha) & -\sin(\beta) \\ \sin(\alpha) & \cos(\alpha) & 0 \\ \sin(\beta)*\cos(\alpha) & -\sin(\beta)*\sin(\alpha) & \cos(\beta) \end{pmatrix} \quad (3)$$

where α is the strike azimuth (for the coordinate system of main stresses α = 0).
Accordingly:

$$\sigma_f = A*\sigma_g*A^T \quad (4)$$

where A^T — transposed matrix A. As a result, σ_f is equal:

$$\sigma_f = \begin{pmatrix} 119.8 & 0 & 71.9 \\ 0 & 161.3 & 0 \\ 71.9 & 0 & 202.8 \end{pmatrix} \quad (5)$$

Since gravity is not directly considered in CFRAC, the stress trends in the fracture-dyke coordinate system must be determined: $\frac{\partial \sigma_{xx}}{\partial z}$ = 12.4 MPa/km, $\frac{\partial \sigma_{yy}}{\partial z}$ = 16.7 MPa/km, $\frac{\partial \sigma_{zz}}{\partial z}$ = 21.0 MPa/km, $\frac{\partial \sigma_{xz}}{\partial z}$ = 7.4 MPa/km. The above stress trends were calculated by numerical differentiation of the stress tensor, using ΔZ increments and assuming that the effective stress in the host rock masses is controlled by hydrostatic water pressure. If magma is considered as the fluid phase controlling the effective stress in the host rock massifs, then the trends of effective stresses in the fracture-fracture coordinate system are: $\frac{\partial \sigma_{xx}}{\partial z}$ = –1.0 MPa/km, $\frac{\partial \sigma_{yy}}{\partial z}$ = –1.3 MPa/km, $\frac{\partial \sigma_{zz}}{\partial z}$ = –1.7 MPa/km, $\frac{\partial \sigma_{xz}}{\partial z}$ = –0.6 MPa/km.

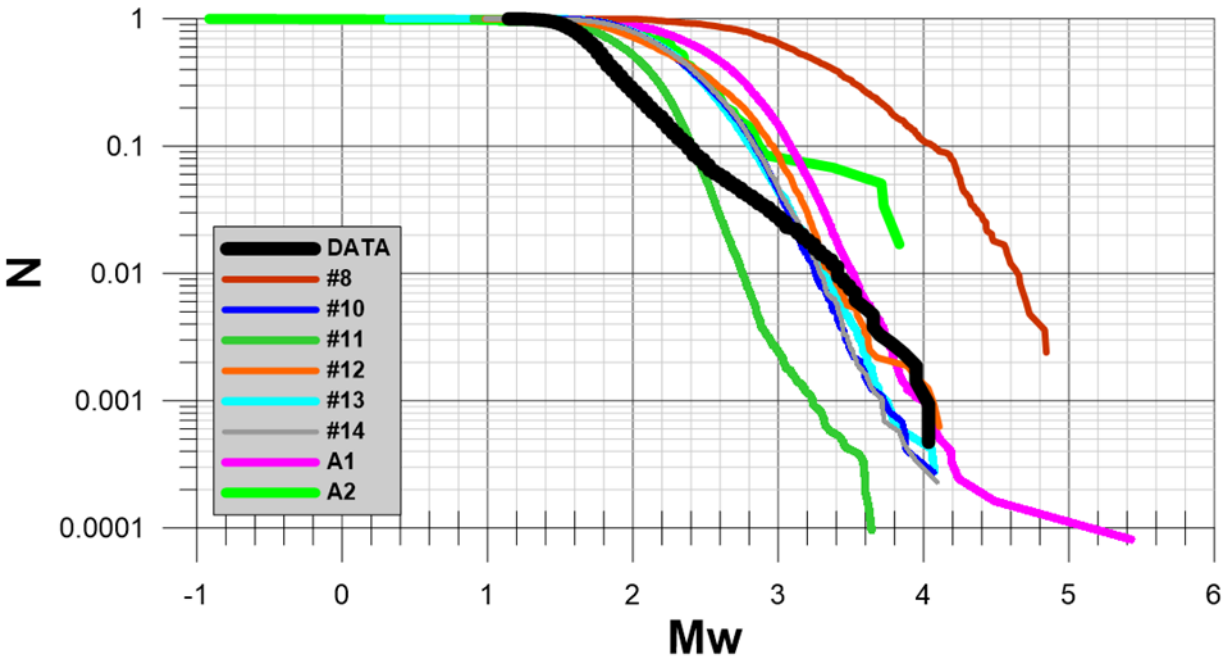

Figure 4: Gutenberg-Richter seismicity diagram: MEQ microearthquake data under Mutnovsky volcano 01.2009-10.2020 and MEQ generated on the hydro-mechanical model (CFRAC) of magma injection into the existing fracture with 30º dip angle (static/dynamic option) for modeling options with hydrostatic water gradient in the host rock masses (modeling scenarios ##8, 10-14, Table 3).
Notes: Mw=exp(2.133+0.063·Ms)-6.205, Ms≤5.5; Mw= exp(-0.109+0.229·Ms)+2.586, Ms≥5.5; Lolli et al, 2014, p.813, Ms=(Ks-4.6)/1.5, Fedotov, 1972, p.67.

Table 2: CFRAC modeling scenarios. Note: Mo, seismic moment (or E –energy) was calculated using relationship (2)

##	Rate, kg/s	μ, Pa·s	P init MPa	G MPa	Area km^2	μu stat	μu dyn	E, m	Time, days	N	Mw max	M_0 N·m (E, J)
1	100	2	78	15000	4 x 4	0.6	0.55	0.01	30	545	4.98	1.39E18
2	100	2	78	15000	4 x 4	0.6	0.55	0.1	30	155	4.99	1.40E18
3	100	2	78	15000	4 x 4	0.6	0.55	1.0	30	119	4.94	1.28E18
4	10	2	78	15000	4 x 4	0.6	0.55	1.0	30	89	4.93	9.74E17
5	10	2	10	15000	4 x 4	0.6	0.55	1.0	30	32	5.01	2.93E17

6	10	2	5	15000	4 x 4	0.6	0.55	1.0	30	31	5.00	2.39E17
7	10	2	20	15000	4 x 4	0.6	0.55	1.0	30	28	4.91	3.33E17
8	100	2	78	1500	4 x 4	0.6	0.55	0.01	30	833	4.84	5.23E17
9	10	2	78	150000	4 x 4	0.6	0.55	1.0	30	79	4.93	9.74E17
10	**2000**	**9e-5**	**78**	**15000**	**4 x 4**	**0.60**	**0.59**	**0.0005**	**1**	**7318**	**4.07**	**7.3E16**
11	2000	9e-5	78	15000	4 x 4	0.60	0.599	0.0005	1	20848	3.64	5.18E16
12	200	9e-5	78	15000	4 x 4	0.60	0.595	0.0005	1	3196	4.11	4.70E16
13	2000	9e-5	78	1500	4 x 4	0.60	0.59	0.0005	1	7153	4.07	7.41E16
14	2000	9e-6	78	15000	4 x 4	0.60	0.59	0.0005	1	8738	4.09	9.08E16
A1	2000	9e-5	10	15000	4 x 4	0.60	0.59	0.0005	1	12316	4.48	3.00E17
A2	2000	9e-5	10	15000	2 x 2	0.60	0.59	0.0005	1	58	3.72	1.39E15
A3	2000	9e-5	10	15000	0.2 x .2	0.60	0.59	0.0005	1	55	3.51	5.32E14

4.2 Modeling Results

Seventeen simulation variants were performed at different values of magma viscosity, magma injection flow rate and time, initial magma pressure in the fracture, difference in static and dynamic friction coefficients, size and initial dyke-fracture opening (Table 1). As a result of modeling, the distributions of the following characteristics in the fracture-dyke were obtained: fluid pressure, normal and shear effective stresses, vectors of shear strains, fracture opening, hypocenters and magnitudes of microearthquakes (MEQ) for different time moments. The goal of the simulation was to obtain the correspondence between the statistics of the observed and model-generated earthquake swarms on the Gutenberg-Richter diagram (Fig. 4).

The simulation results for the variants (#1-9, Table 1) show that changes in the magma injection flow rate, initial magma pressure in the fracture, shear modulus, and initial fracture opening do not significantly affect the values of the model distribution of earthquake magnitudes Mw, which seemed on average to be one order greater than actually observed.

Results of modeling by variants (#10-14, A1-A3, Table 1) allowed us to discover that when the difference between μdynamic (dynamic friction coefficient of fracture walls) and μstatic (static friction coefficient of fracture walls) decreased to 0.01, the values of model-generated Mw earthquake amplitudes decreased and the values of observed and model-generated earthquakes became consistent (Fig. 4). At the same time, the number of model-generated earthquakes during a single magma injection increased to the first thousand (#10,12-14, Table 1) or to the first tens of thousands (#11, A1, Table 1), although the actually recorded maximum number of MEQ in one cluster is 61. Decreasing the size of the fracture-fault (#A1-A3, Table 1) leads to a significant decrease in the number of earthquakes (up to the first tens) and their magnitudes.

The results of CFRAC modeling variant #10 (Table 1) shows fracture opening occurs upwards and is characterized by fluid pressure from 98 to 118 MPa, effective normal stress drops to zero in the opening zone, shear deformations during injection generate 7318 microearthquakes with magnitude Mw up to 4.07 distributed throughout the fracture plane. Opening of the fracture reaches 0.05 m (in the upper part) and 0.0003 m (in the central part). The hanging block of the fracture moves upward relative to the lying block (thrust). In the central part, the shear displacements reach 9 m. The effect of opening the upper part of the fracture-dyke during magma injection, while the lower part of the fracture remains closed, obtained from the model, is exceptionally important. This corresponds to the observed positioning of seismogenic fracture-gaps in the NE sector of Mutnovsky volcano with a shift relative to the volcano magma feeder channels against the dip direction and along the strike of geomechanically active shear fracture-dykes in accordance with the values of magma fluid pressure gradients of 14.0 MPa/km and the effective stress ($\frac{\partial \sigma_{zz}}{\partial z}$ = 21.0 MPa/km) in the coordinate system referenced to the plane of the considered fracture-dykes (see above).

Note also that when the mass flow rate (volume) of magma injection is changed and the values of the other parameters are fixed, the total seismic energy released increases significantly (comparison of variants #3 and #4, #10 and #12). This suggests the possibility of the existence of an empirical dependence between the volume of magma injection and the total seismic energy released in this case.

5. CONCLUSION

5.1 The granite porphyry system consisted of three main parts based on their texture (the crystalline, porphyritic, and silicified). The granite–porphyry can be used as a natural analog for the supercritical geothermal structure. The structure was given as the crystalline granodiorites as the heat source according to that placed at ~8–11 km depth (~200–300 MPa according to Al–in–Hbl geobarometry) with a temperature of ~531–793°C (Ti–in–Qtz geothermometry). Porphyritic granodiorite breached by the vein and veinlets existed as the supercritical geothermal reservoir at ~7–8 km (~175–200 MPa). Silicified zone granite was carried out as the caprock right above

the reservoir at ~6.5−7 km depth (~175 MPa) with a temperature of ~430ºC from Ti−in−Qtz geothermometry. The high−temperature hydrothermal quartz was formed during self−sealing and become the cap−rock for a supercritical geothermal system, then accomp anied by the formation of an irregular quartz vein. The straight quartz vein followed the hydrothermal breccia marked the transitions of lithostatic to hydrostatic pressure. The highly silicified zone on top of granodiorite intrusion in granite–porphyry systems provide valuable evidence of cap rocks and thus extends a suitable natural analog of supercritical geothermal systems.

5.2 Mutnovsky volcano low angle dykes injections were reproduced by hydromechanical simulation using CFRAC, modeling results matches with MEQ's statistics observed. Nevertheless, the following results obtained in the hydromechanical model are required to be clarified: (1) large shear displacements (up to 9 m) of fracs; (2) relatively small opening of fracs (less than 0.05 m); (3) a large number of MEQ's generated in a single frac. Model sensitivity to a friction coefficient (μstatic), defined as 0.6 in hydromechanical model, was not investigated yet. Thus, friction coefficient may be trialed for these purposes in a future modeling study. Higher values of friction coefficient may point on occurrence of a more plastic conditions in a NE Mutnovsky magma injection zone, implying some kind of supercritical geothermal resources may exist there.

ACKNOWLEDGEMENT

NEDO (New Energy and Industrial Technology Development Organization) and JSPS (Japan Society for the Promotion of Science: Japan-Russia Research Collaboration) financially supported the supercritical geothermal project. This study was also funded by RFBR and JSPS according to research project # 21-55-50003. We would like to say thanks to all members of the research project. Authors also express gratitude to M. McClure and R. Horne for CFRAC permission to use.

Author Contributions: Conceptualization, Mutnovsky MEQ's data curation and analysis, hydromechanical simulation, writing—original draft preparation: A.K.; Conceptualization, introduction, geological background, supercritical geothermal resources, writing—original draft preparation: N.T. All authors have read and agreed to the published version of the manuscript.

REFERENCES

Akinfiev, N.N., Diamond, L.W., 2009. A simple predictive model of quartz solubility in water-salt-CO2 systems at temperatures up to 1000°C and pressures up to 1000 MPa. Geochim. Cosmochim. Acta 73, 1597–1608. https://doi.org/10.1016/j.gca.2008.12.011

Amagai, et al., 2019, Silica nanoparticles produced by explosive flash vaporization during earthquakes, Scientific Reports, 10.1038/s41598-019-46320-7

Amanda et al., 2019, Evaluation of Caldera Hosted Geothermal Potential during Volcanism and Magnetism in Subduction System, NE Japan, Geofluids, 10.1155/2019/3031586

Asanuma H., Mogi T., Tsuchiya N., Watanabe N., Naganawa S., Ogawa Y., Fujimitsu Y., Kajiwara T., Osato K., Shimada K., Horimoto S., Sato T.,Yamada S., and Watanabe K.Japanese Supercritical Geothermal Project for Drastic Increase of Geothermal Power Generation in 2050 //Proceedings World Geothermal Congress 2020+1 Reykjavik, Iceland, April - October 2021

Chubarova O.S., Gusev A.A., Chebrov V.N. The Ground Motion Excited by The Olyutorskii Earthquake of April 20, 2006 And by Its Aftershocks Based on Digital Recordings // Journal of Volcanology and Seismology. 2010. T. 4. № 2. C. 126-138).

Eichelberger J., Kiryukhin A., Mollo S., Tsuchiya N. and Villeneuve M. Exploring and Modeling the Magma–Hydrothermal Regime. Geosciences 2020, 10, 0234; doi:10.3390/geosciences10060234

Fedotov S.A. Energetic classification of the Kurilo-Kamchatka earthquakes and the problem of magnitudes. Moscow: Nauka., 1972. 116 c. (in Russian)

Fedotov S.A., Solomatin A.V. Long-term seismic forecast for the Kurilo-Kamchatka arc for VI 2019 - V 2024.... // Volcanology and Seismology. 2019. № 6. C. 6-22

Fournier, R.O., 1999, Hydrothermal Processes related to movement of fluid from plastic into brittle rock in the magmatic–epithermal environment. Econ. Geol. 94, 1193–1211.

Kiryukhin, A.V., 1996. Modeling studies: the Dachny geothermal reservoir, Kamchatka, Russia. Geothermics 25 (#1), 63–90.

Kiryukhin A., Norbeck J. Analysis of Magma Injection Beneath an Active Volcano Using a Hydromechanical Numerical Model. Proc. 42nd Workshop on Geothermal Reservoir Engineering Stanford University, Stanford, California, February 13–15, 2017. P. 740–747.

Kiryukhin A., Polyakov A., Kiryukhin P. Analysis of Magma Injections Beneath Mutnovsky Volcano (Kamchatka) // PROCEEDINGS, 43rd Workshop on Geothermal Reservoir Engineering Stanford University, Stanford, California, February 12-14, 2018, p. 658-666.

Kiryukhin A. V., Polyakov A. Y., Usacheva O. O., Kiryukhin P. A. Th ermal-Permeability Structure and Recharge Conditions of the Mutnovsky High Temperature Geothermal Field (Kamchatka, Russia). J. of Volcanology and Geothermal Research, 2018. Vol. 356. P. 36–55.

Kiryukhin A.V. Geothermofluidomechanics of hydrothermal, volcanic and hydrocarbon systems// St. Petersburg: Eko-Vector I-P, 2020. 431 p. (in Russian) https://www.elibrary.ru/download/elibrary_45739830_67113473.pdf

Kiryukhin P.A., Kiryukhin A.V. Frac-Digger. Certificate of state registration of computer programs # 2016612168 of 21.06.2016.

Kiryukhin A.V., Polyakov A.Y., Voronin P.O., Zhuravlev N.B., Usacheva O.O, Solomatin A.V. Magma Fracking and Production Reservoirs Beneath and Adjacent to Mutnovsky Volcano Based on Seismic Data and Hydrothermal Activity // submitted to Geothermics, 2021

Lolli B., Gasperini P., Vannucci G. Empirical conversion between teleseismic magnitudes (m_b and M_s) and moment magnitude (M_w) at the Global, Euro-Mediterranean and Italian scale Geophysical Journal International, Volume 199, Issue 2, November 2014, Pages 805–828, https://doi.org/10.1093/gji/ggu264

McClure M. W. Modeling and characterization of hydraulic stimulation and induced seismicity in geothermal and shale gas reservoirs, PhD Th esis, Stanford University, Stanford, California, 2012.

McClure M. CFRAC (version 1.2) Complex Fracturing ReseArch Code User›s Guide (version 20), December 2014. 88 p.

McClure M. W., Horne R. N. Discrete Fracture Network Modeling of Hydraulic Stimulation:Coupling Flow and Geomechanics, Springer, 2013. https://doi.org/10.1007/978-3-319-00383-2.

Muraoka, H., Uchida, T., Sasada, M., Yagi, M., Akaku, K., Sasaki, M., Yasukawa, K., Miyazaki, S.I., Doi, N., Saito, S., Sato, K., Tanaka, S., 1998. Deep geothermal resources survey program: Igneous, metamorphic and hydrothermal processes in a well encountering 500°C at 3729 m depth, Kakkonda, Japan. Geothermics 27, 507–534. https://doi.org/10.1016/S0375-6505(98)00031-5

Reinsch, T., Dobson, P., Asanuma, H., Huenges, E., Poletto, F., Sanjuan, B., 2017. Utilizing supercritical geothermal systems: a review of past ventures and ongoing research activities. Geotherm. Energy 5, 1–25. https://doi.org/10.1186/s40517-017-0075-y

Saishu, et al., 2014, The significance of silica precipitation on the formation of the permeable–impermeable boundary within Earth's crust, Terra Nova, 26, 253-259. 10.1111/ter.12093

Selyangin, O.B., 1993. Mutnovsky volcano, Kamchatka: new evidence on structure, evolution,and future activity. J. Volcanol. Seismol. 15, 17–38.

Selyangin, O.B., 2009. Wonderful World of Mutnovsky and Gorely Volcanoes: Volcanologic and Traveller's Guide. Novaja kniga, Petropavlovsk-Kamchatsky (108 pp.).

Simon A., Yogodzinski G.M., Robertson K., Smith E., Selyangin O., Kiryukhin A., Mulcahy S.R., Walker J.D., 2014. Evolution and genesis of volcanic rocks from Mutnovsky volcano, Kamchatka. J. Volcanol. Geotherm. Res. 286, 116–137.

Tsuchiya N. Geological Model and Potential of Supercritical Geothermal Reservoir//Proceedings World Geothermal Congress 2020+1 Reykjavik, Iceland, April - October 2021

Tsuchiya et. al., 2016, Supercritical geothermal reservoir revealed by a granite–porphyry system, Geothermics, 63, 182-194. 10.1016/j.geothermics.2015.12.011

Tsuchiya N. and Amanda F. // High Temperature Silicified Zone as a Cap-Rock for Supercritical Geothermal Fluids // PROCEEDINGS, Geothermal Volcanology Workshop Petropavlovsk-Kamchatsky, Russia, September 06-11, 2021

Watanabe, et al., 2017, Potentially exploitable supercritical geothermal resources in the ductile crust, Nature Geoscience, 10.1038/NGEO2879

Watanabe, et al., 2019 Cloud-fracture networks as a means of accessing superhot geothermal energy, Scientific Reports, 10.1038/s41598-018-37634-z